



OPEN

Broadband high-resolution molecular spectroscopy with interleaved mid-infrared frequency combs

A. V. Muraviev, D. Konnov & K. L. Vodopyanov

Traditionally, there has been a trade-off in spectroscopic measurements between high resolution, broadband coverage, and acquisition time. Originally envisioned for precision spectroscopy of the hydrogen atom in the ultraviolet, optical frequency combs are now commonly used for probing molecular ro-vibrational transitions throughout broad spectral bands in the mid-infrared providing superior resolution, speed, and the capability of referencing to the primary frequency standards. Here we demonstrate the acquisition of 2.5 million spectral data points over the continuous wavelength range of 3.17–5.13 μm (frequency span 1200 cm^{-1} , sampling point spacing 13–21 MHz), via interleaving comb-tooth-resolved spectra acquired with a highly-coherent broadband dual-frequency-comb system based on optical subharmonic generation. With the original comb-line spacing of 115 MHz, overlaying eight spectra with gradually shifted comb lines we fully resolve the amplitude and phase spectra of molecules with narrow Doppler lines, such as carbon disulfide (CS_2) and its three isotopologues.

Coherent laser beams in the 3 to 20 μm mid-infrared (mid-IR) region provide a unique prospect for sensing molecules through addressing their strongest absorption bands. Thanks to their coherent and broadband nature, optical frequency combs can probe molecular signatures over an extensive (e.g. more than an octave) spectral span simultaneously^{1,2}. When one (or several) of the comb teeth is phase locked to a narrow-linewidth reference laser(s), frequency comb spectroscopy can provide the spectral resolution, which is on par with tunable laser spectroscopy—limited only by the absolute comb-tooth linewidth. However, comb spectroscopy has a strong advantage of massive parallelism of data collection and, most importantly, the absolute optical frequency referencing to an accurate external standard (e.g. atomic clock) over the whole spectral span of the comb. Combs with high degree of phase coherence can be used in the dual comb spectroscopy (DCS)—one of the most advanced spectroscopic techniques. In a dual-comb spectrometer, a sensing comb is transmitted through a sample and then multi-heterodyned against a local oscillator (LO) comb which has a repetition rate f_r that differs by a small fraction Δf_r from that of the sensing comb. Compared to classical Fourier transform infrared spectroscopy, DCS demonstrates remarkable improvement of spectral resolution, data acquisition speed, and sensitivity, all at the same time³.

With a high degree of mutual coherence between the two combs in a DCS system, it is possible to obtain comb-tooth resolved spectra^{3–5}. Using DCS in the near-IR (comb span 1.36–1.69 μm), Zolot et al. resolved the phase and amplitude of over 400,000 individual comb modes at a mode spacing of 100 MHz⁵. In the mid-IR, by utilizing frequency combs near 3.3 μm (spectral span 12 cm^{-1}) achieved by applying a nonlinear mixing step to near-IR combs produced by electro-optic modulation (EOM) technique, Yan et al. resolved 1,200 comb lines with the line spacing of 300 MHz⁶. Subsequently, two groups demonstrated comb-tooth resolved spectra over a broad span of frequencies: Ycas et al. resolved 270,000 comb lines between 2.6 and 5.2 μm in four overlapping spectral sequences (with mode spacing 200 MHz and a combined frequency span 1800 cm^{-1})⁷, and Muraviev et al. resolved 350,000 comb lines with a finesse of 4,000 within a single frequency comb spanning 3.1–5.5- μm (mode spacing 115 MHz, frequency span 1400 cm^{-1}) and also demonstrated simultaneous detection of more than 20 molecular species in a mixture of gases⁸.

Once comb teeth are resolved, the spectral resolution is defined by the comb tooth linewidth, which can be orders of magnitude narrower than the comb-line spacing. Then, high-resolution measurements can be

CREOL, College of Optics and Photonics, University of Central Florida, Orlando, FL 32816, USA. email: vodopyanov@creol.ucf.edu

implemented by interleaving spectra taken with discretely stepped—either comb repetition rate f_r or carrier-envelope offset (CEO) frequency f_{ceo} ^{2,9–13}. For example, using a near-IR comb (span of 1.5–1.64 μm) and a mechanical Fourier transform spectrometer with mode-resolving capability, Rutkowski et al. performed measurements, which yielded 2.4 million sampling points with a step of 20 kHz—performed by interleaving spectra with frequency-shifted comb lines¹⁴. In the mid-IR, Baumann et al. used difference frequency combs near 3.4 μm (spectral span 30 cm^{-1}), to attain a high-resolution spectrum of methane, by interleaving spectra acquired by shifting the combs by 25 MHz—one-quarter of the 100-MHz comb-tooth spacing¹⁰. Using quantum cascade laser (QCL) combs, Villares et al. performed DCS measurements near 7 μm (span 16 cm^{-1}) with the sampling point spacing that was improved from the original comb-tooth spacing of 7.5 GHz to 80 MHz by frequency sweeping the combs via QCL current modulation¹⁵. Similarly, by utilizing dual QCL combs near 8.3 μm (span 55 cm^{-1}), Gianella et al. achieved an improvement in the sampling point spacing from 9.8 GHz to 30 MHz by sweeping the frequencies of both the sensing and LO combs via synchronized current modulation¹⁶. In the two above QCL scenarios the combs were free running with no absolute optical frequency referencing; rather, the frequency scale was calibrated by comparing the spectra with the HITRAN database¹⁷. Overall, the spectral width of mid-IR measurements with interleaved combs does not exceed 60 cm^{-1} with one exception of a silicon microresonator comb with a span of 3–3.5 μm that was scanned with a step of 80 MHz via tuning both the pump laser frequency and the cavity resonance. However, the comb lines were scanned over 16 GHz—a small portion of the 127-GHz mode spacing¹⁸.

One of the challenges of DCS is to get high spectral resolution over a broad bandwidth—required, for example, in applications related to multi-species detection in gas mixtures. To achieve high resolution, one needs long mutual coherence time between the two combs³. If the combs are not fully locked, one can track the relative phase drifts and correct for these in real time, at the expense of having two stable continuous-wave reference lasers, as has been demonstrated in the near-IR^{19–21}, or perform phase correction by a posteriori data processing, as has been shown in the THz and mid-IR ranges^{22,23}. However, both of these methods lack the absolute frequency referencing—a setup needs to be calibrated using, for example, a well-known gas absorption feature.

Degenerate (subharmonic) optical parametric oscillators (OPOs) pumped by mode-locked lasers are noteworthy sources of broadband mid-IR frequency combs^{24–28} and are now used in spectroscopic studies^{8,29,30}, random number generation³¹, and in coherent Ising machines³². Their key benefits are: low (~ 10 mW) oscillation threshold, extremely broad bandwidth, good stability when the cavity is actively locked to resonance, and high conversion efficiency that can exceed 50%³³. It has been established that a subharmonic OPO is an ideal coherent frequency divider without any excess phase noise, which rigorously both coherently down-converts and augments the spectrum of the pump frequency comb^{34–37}.

Here we demonstrate, using a highly-coherent subharmonic DCS system, the acquisition of > 2.5 million spectral data points over the whole (no gaps) spectrum of 3.17–5.13 μm (frequency span 1200 cm^{-1} , 36 THz). The sampling density achieved by interleaving comb-line resolved spectra from consecutively shifted combs was sufficient to fully resolve Doppler-broadened absorption bands of several heavy molecules, such as CS_2 and OCS, with the main effort focused on CS_2 . Its choice was motivated (i) by its importance for atmospheric chemistry³⁸, astrophysics³⁹, and medical diagnostics^{40,41}, and (ii) by the fact that the accurate high-resolution spectroscopic data for CS_2 in the mid-IR range were not yet available.

Experiment

Dual-comb setup. Our dual-comb system used a pair of subharmonic OPOs based on orientation-patterned GaAs (OP-GaAs) crystal as a $\chi^{(2)}$ gain medium, pumped by a highly coherent twin Tm-fiber frequency comb system with a central wavelength of 1.93 μm , pulse duration of 90 fs, repetition rate $f_r \approx 115$ MHz, and the average power of 300 mW for each laser⁸.

In order to stabilize Tm laser frequency combs, a portion of each laser's output was used to generate a supercontinuum (SC) in a nonlinear silica fiber. While the 1.1- μm and 2.2- μm SC components were used to stabilize the CEO frequency via $f-2f$ interferometry, the component near 1.56 μm was utilized to obtain beat notes with a narrow-linewidth reference diode laser from Redfern Integrated Optics (RIO). Each OPO (Fig. 1) had a ring-cavity bow-tie design with low cavity group delay dispersion (GDD) achieved by (i) using low-dispersion mirrors, (ii) a thin (0.5-mm-long) OP-GaAs crystal, and (iii) an intracavity wedge made of CaF_2 for GDD compensation^{8,36}. The instantaneous spectral coverage of the DCS system was 3.17–5.13 μm (span 1200 cm^{-1}) at -10 dB and 3.08–5.40 μm (span 1400 cm^{-1}) at -20 dB level. The mutual coherence time between the two subharmonic OPOs was previously measured to be as long as 40 s⁸. Our data acquisition electronics and frequency counters were referenced to a Rb atomic clock, which provided $\sim 10^{-10}$ absolute accuracy of the frequency readings.

Spectroscopic measurements with interleaved combs. We used a one-sided DCS configuration (Fig. 1), where only one ('sensing') comb passes through the gas sample. This eliminates the ambiguity of the double-sided scheme, where an absorption profile is probed by both comb lines simultaneously and allows phase spectrum measurement. For absorption measurements we used a multipass gas cell (AMAC-76LW from Aerodyne Research) with 76-m path length and 0.5-L volume. The sensing and LO combs were combined and sent to an infrared detector (InSb from Kolmar, 77 K, 60 MHz) whose output was fed into a 16-bit analogue-to-digital converter (AlazarTech, ATS9626). We used a wedge made of a dielectric (CaF_2) in the LO channel (Fig. 1) to compensate the dispersion of the multipass cell windows. This did not affect the measured spectrum but made the interferogram sharper, which helped to minimize a jitter in the coherent interferogram averaging process.

First, we demonstrated that an enormous amount of spectral information can be obtained by spectral interleaving over our broadest comb span of 3.17–5.13 μm . The repetition rate offset between the two combs was set to $\Delta f_r = 138.5$ Hz, which allowed mapping the whole 1200 cm^{-1} -wide optical spectrum into a radiofrequency

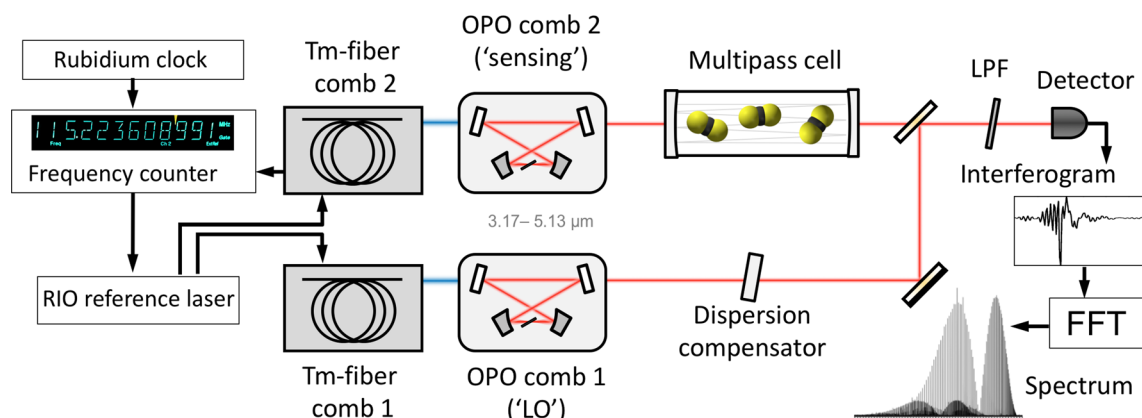


Figure 1. Schematic of the dual-comb spectroscopy setup. LPF, longwave pass filter.

(RF) range of 1–48 MHz ($< f_r/2$, see [Methods](#)). For each comb-line-resolved measurement, we coherently averaged data streams consisting of 10 centerbursts spaced by $1/\Delta f_r \approx 7.2$ ms, with the coherent averaging time from a few seconds to several hours. For each data stream, the data acquisition process was triggered by the sharp central spike of the interferogram, which provided good repeatability of the waveforms and allowed long (for at least > 10 h) coherent averaging without applying any phase correction procedures. After Fourier transforming the time-domain signal and RF-to-optical frequency up-scaling (see [Methods](#)) we obtained a comb-tooth-resolved optical spectrum. By a controlled stepping the optical frequency of the reference RIO laser (see [Methods](#)), the comb lines were tuned, thus filling 115-MHz-wide gaps between the comb lines. To fully resolve Doppler-broadened linewidths of species with relatively high molecular weight, such as CS_2 (Doppler linewidth ~ 90 MHz), we elected to interleave eight comb-line-resolved spectra.

Figure 2a shows the entire comb-tooth-resolved optical spectrum, consisting of more than 2.5 million comb lines obtained from eight interleaved spectra. The total averaging time was 48 min (6 min for each frequency-shifted measurement). The magnified spectrum, Fig. 2b–d, reveals narrow (Doppler-broadened) absorption dips due to the molecules present in the gas cell (CS_2 , CO), and Fig. 2e shows phases for individual comb lines, modified by molecular resonances.

The comb-line-resolved spectra were obtained in the following way. A digitized (8-ns point spacing, 16-bit vertical resolution) averaged waveform containing N_c centerbursts was resampled to get an integer number of data points M_p (typically expressed as a power of 2) per time interval that is equal to $1/\Delta f_r$. (In our experiment Δf_r is known with a fractional accuracy of better than 10^{-9} , see [Methods](#).) After a Fourier transform, one gets $M_p \times N_c$ spectral points, where $N_c - 1$ points out of N_c are zero (at the noise level), and only one point is non-zero with its value being proportional to the amplitude of a comb line. This may be seen in the zoomed mode-resolved spectrum of Fig. 2d (left panel, black color), which was obtained from a waveform containing $N_c = 10$ centerbursts. As a result of this procedure, the center frequency for each comb line is well-defined with the fractional uncertainty for the absolute value of $\sim 7.8 \times 10^{-10}$ —through a unique RF-to-optical mapping (see [Methods](#)).

Results

CS_2 molecule. For high-precision measurements of the $\nu_1 + \nu_3$ band of CS_2 , our spectral span was narrowed down to approximately $2030\text{--}2300\text{ cm}^{-1}$ (4.3–4.9 μm ; ~ 10 -dB level)—achieved by a combination of tweaking the OPO cavities and using a longpass optical filter (the reduced spectrum is shown in the inset to Fig. 3a). The spectral narrowing allowed to increase the signal-to-noise ratio (SNR)¹¹ and also increase Δf_r by a factor of four, to $\Delta f_r = 554$ Hz. With the acquisition time of ~ 200 min for each frequency-shifted spectrum, we reached the fractional standard deviation for the comb-line amplitude of 1.5×10^{-4} (SNR 6.6×10^3). With the average SNR of 4.4×10^3 over the central (~ 4.5 -dB level) $\approx 50,000$ modes of the comb (span $\approx 200\text{ cm}^{-1}$), the DCS figure of merit (FOM), identified in¹¹ as $\text{SNR} \times M/\sqrt{\tau}$ (M is the number of modes and is τ the averaging time), we get $\text{FOM} = 2.1 \times 10^6\text{ Hz}^{1/2}$.

The gas mixture in the multipass cell had a total pressure of 6.03 mbar and contained a trace amount of CS_2 at a concentration of 94.6 ± 3 ppm (part-per-million by volume), with n-hexane and room air as buffer gases in similar proportions (see [Methods](#)). Figure 3a,b show the absorbance ($A = -\ln(T/T_0)$, where T is the power transmission with, and T_0 —without a sample) and phase spectrum corresponding to the $\nu_1 + \nu_3$ absorption band of CS_2 . A magnified view of the CS_2 absorbance and phase is given in Figs. 3c,d. The baseline for each interleaved spectrum was obtained by the asymmetric least squares smoothing algorithm based on the Whittaker smoother⁴² with the smoothing parameter that was optimized in such a way that the deviation from the actual data (sufficiently away from a line center) did not exceed the local noise level. Due to the low pressure and high resolution, the spectral lines of other molecules— H_2O , CO_2 , CO, and N_2O —present in the gas mixture due to the room air, practically didn't interfere with the CS_2 lines. On the other hand, n-hexane, used as a solvent for CS_2 , does not have any characteristic absorption features across the spectral span used here, and gave a very smooth absorption offset. The spectra were obtained from eight interleaved comb-line resolved measurements. Every data point represents a comb line with a known absolute frequency (see [Methods](#)). The distance between the

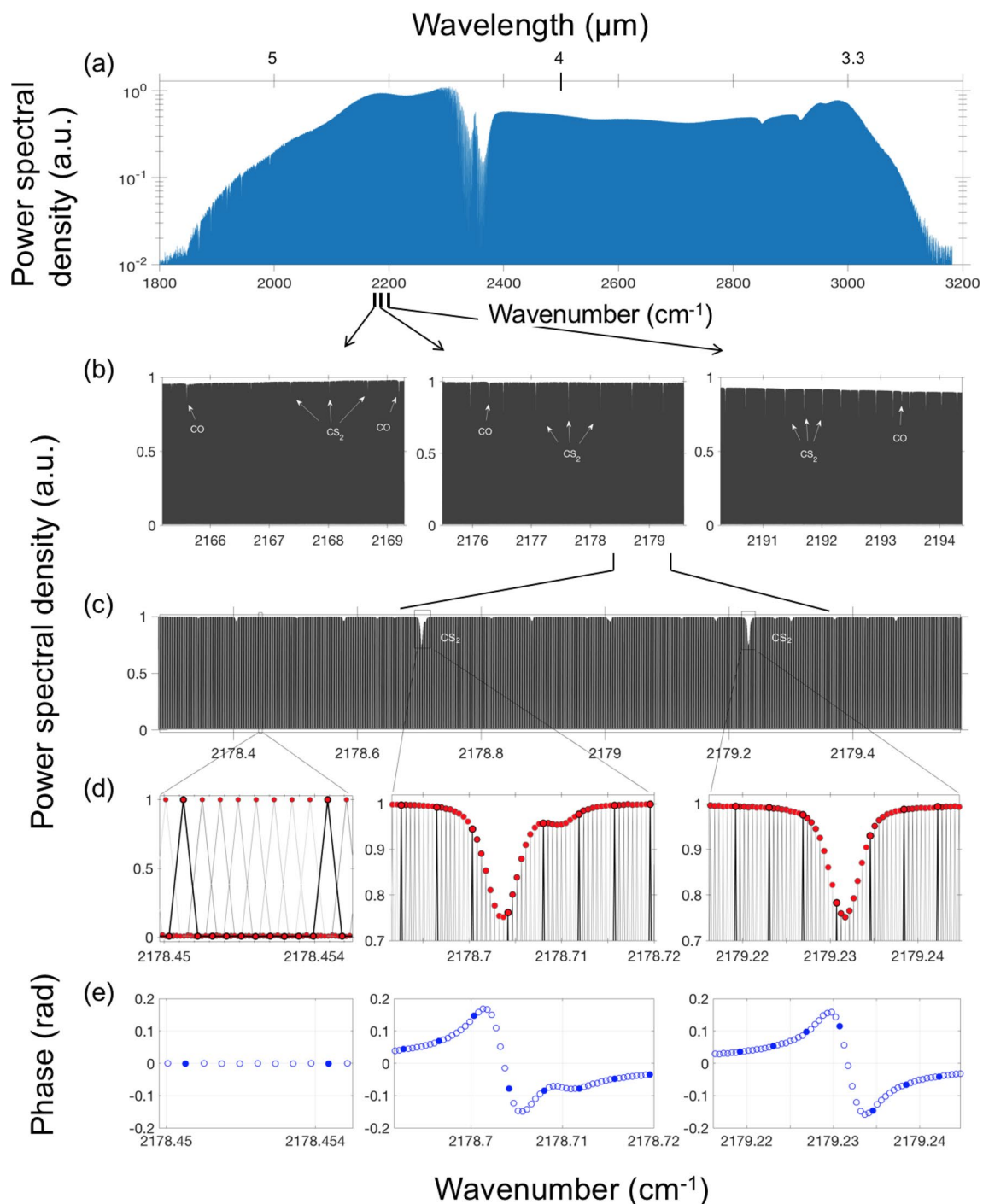


Figure 2. (a) Combined mode-resolved spectrum (log-scale) containing >2.5 million comb lines (-10 -dB level), obtained by eight interleaved measurements. The broad dips in the spectrum are due to the atmospheric absorption (H_2O , CO_2) outside the gas cell. (b,c) Magnified view of the spectrum showing narrow features due to molecular absorption inside the cell. (d,e) Further magnification shows amplitudes and phases for the individual interleaved comb lines spaced by 14.4 MHz. Features shown in black in (d) and filled circles in (e) correspond to the original comb-line spacing of 115 MHz.

sampling points is 14.4 MHz—about $1/8$ of the original comb-line spacing (115 MHz)—appears to be adequate for resolving the CS_2 Doppler broadened absorption lines.

Figure 4 shows the absorbance spectrum of CS_2 plotted on a log-scale that allows to see the weaker bands. For better visibility of the CS_2 spectrum, the lines of CO and N_2O present in the mixture due to the room air were digitally subtracted via HITRAN simulations using concentration as the only fitting parameter. This was also used to verify the absolute accuracy of our frequency readings: the positions of the CO and N_2O peaks deviated from those obtained from HITRAN by less than 1 MHz and allowed clean removal of these peaks. Additionally,

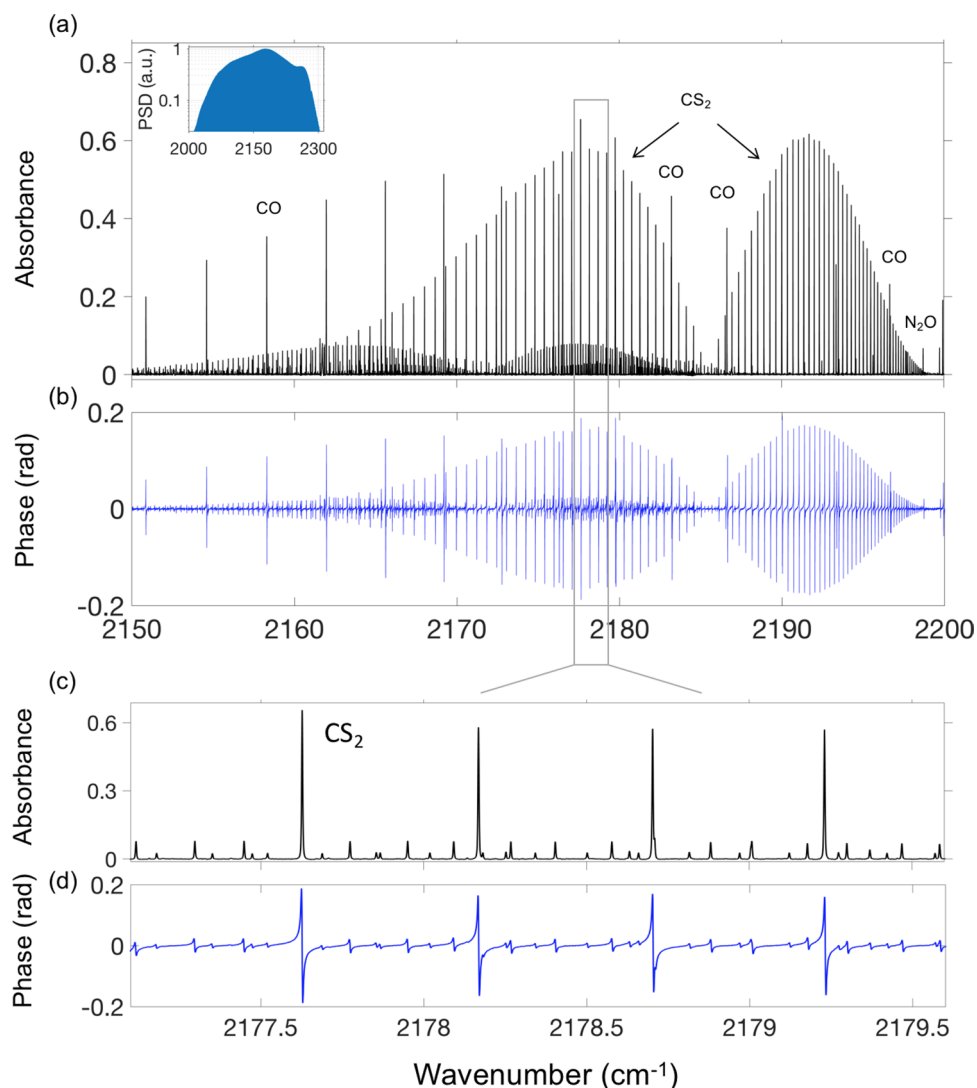


Figure 3. (a,b) Absorbance ($= -\ln(T/T_0)$) and phase spectra for the $\nu_1 + \nu_3$ band of CS_2 obtained at 14.4-MHz spectral point spacing. (c,d) Magnified view of the CS_2 absorbance and phase. The spectral peaks of CO and N_2O in (a,b) are due to the room air in the cell. Inset: Reduced comb spectrum (log-scale) used in this experiment. PSD, power spectral density.

few slices between 2135 and 2165 cm^{-1} —corresponding to strong peaks of water vapor outside the gas cell—were manually cut out in Fig. 4.

The high resolution and long coherent averaging allowed us to identify 981 spectral lines of the $\nu_1 + \nu_3$ absorption band of CS_2 . In fact, because of the low noise of the baseline, we were able to detect CS_2 lines that were about 10^3 times weaker than the strongest ones (see the inset to Fig. 4). In addition to the main molecule, we were able to resolve the spectra of three isotopologues ($^{34}\text{S}^{12}\text{C}^{32}\text{S}$, $^{33}\text{S}^{12}\text{C}^{32}\text{S}$, and $^{32}\text{S}^{13}\text{C}^{32}\text{S}$), as well as the spectra of seven hot bands due to transitions from the thermally excited vibrational states, labelled in Fig. 4. The inset shows the two peaks corresponding to the low-abundance ^{33}S isotope ($\sim 0.8\%$ with respect to ^{32}S), along with the two peaks for the main molecule. More details on our CS_2 measurements, including line lists and the interpretation of the bands can be found in⁴³.

OCS molecule. Figure 5 presents the portion of the spectrum (absorbance and phase) from the same experiment that reveals the presence of trace amounts of carbonyl sulfide (OCS) molecule, although this molecule was not originally present in the gas mixture. The plot also shows the simulated (HITRAN) spectrum for the asymmetric ν_3 stretch of OCS. From the known absorption cross section of OCS, its concentration was evaluated to be 1.75 ppm. Our repeated measurements revealed that the OCS concentration kept rising at a rate of approximately 15% per day, while the concentration of CS_2 was decreasing at a rate of 0.5–0.7% per day. We hypothesize that the emergence of OCS is due to a chemical oxidation reaction of CS_2 in the presence of O_2 in the gas cell⁴⁴.

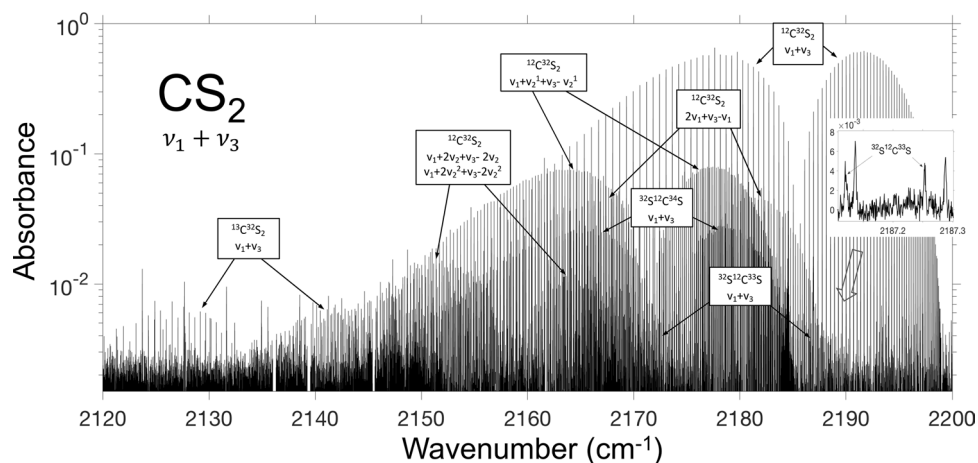


Figure 4. Log-scale spectrum corresponding to the $\nu_1 + \nu_3$ band of CS_2 that include: bands due to isotopes: ^{34}S , ^{33}S , and ^{13}C and hot bands from the thermally excited vibrational states ν_1 and ν_2 . The inset shows two peaks due to the low-abundance ^{33}S isotope. For better visibility of the spectrum, the CO and N_2O lines were digitally subtracted via HITRAN-based simulations. Also, few slices between 2135 and 2165 cm^{-1} corresponding to strong water absorption outside the gas cell were manually cut out.

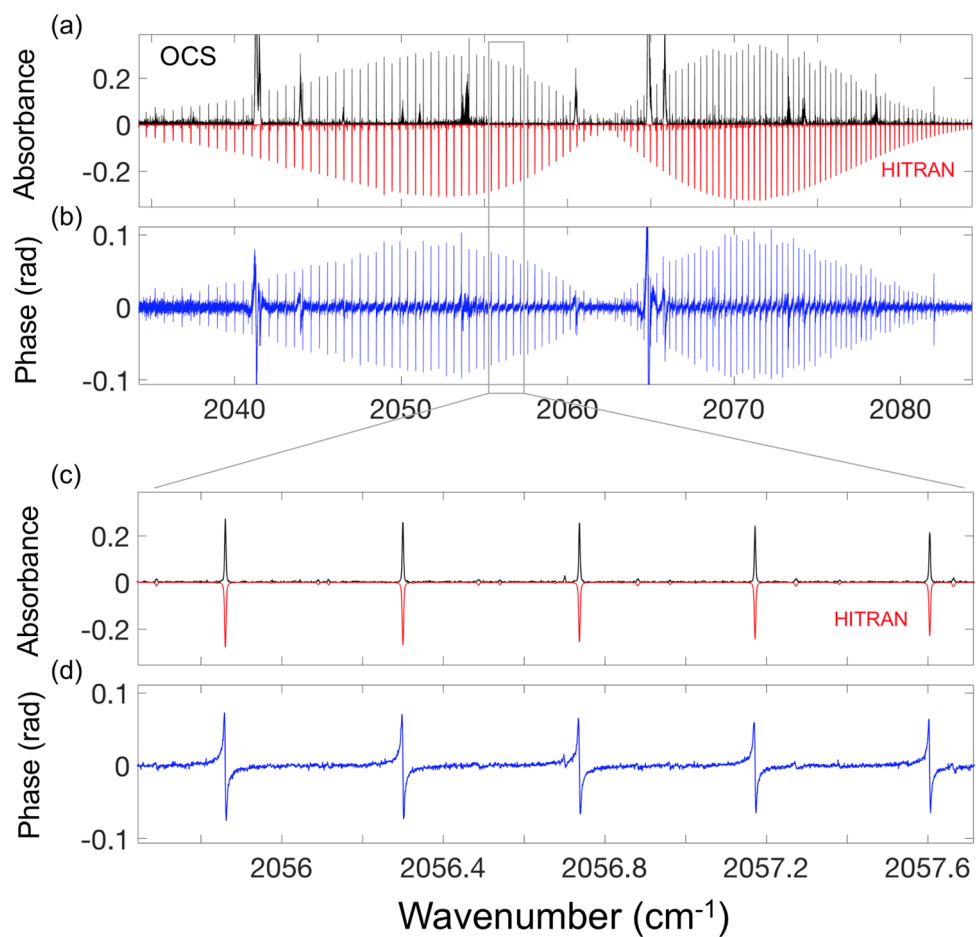


Figure 5. (a) Absorbance and (b) phase spectrum for the ν_3 asymmetric band of OCS . The noise features (e.g. at 2041, 2065 cm^{-1} etc.) are related to strong (and broad) water absorption lines outside the gas cell. (c,d) Expanded OCS spectrum for the absorbance and phase. Shown in (a,c) are simulated HITRAN-based absorbance spectra, inverted for clarity.

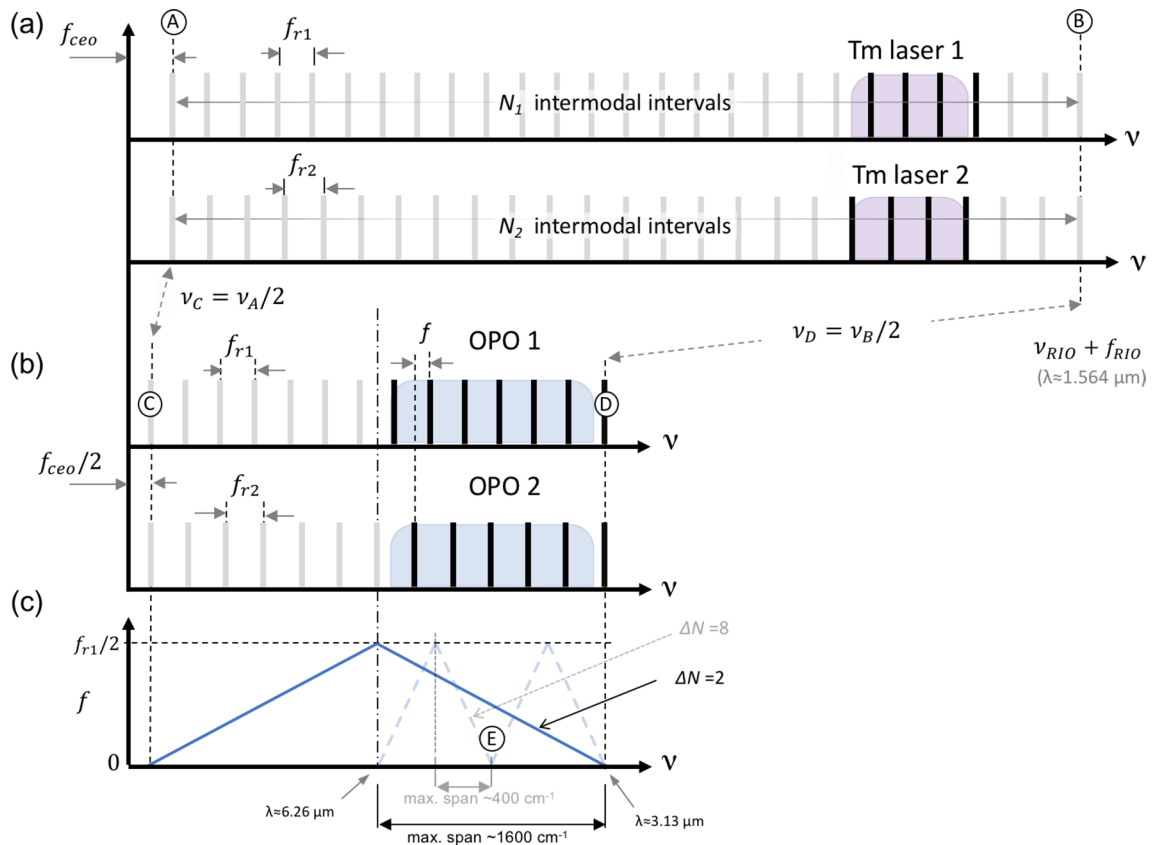


Figure 6. (a) Comb lines extrapolated to zero optical frequency ν for the two Tm-fiber pump lasers, with the repetition rates f_{r1} and f_{r2} respectively. The Tm combs are f_{ceo} stabilized and phase locked to a common narrow-band ‘RIO’ laser ($\lambda \approx 1.564 \mu\text{m}$) so that their teeth overlap at the two lock points ‘A’ and ‘B’. (b) The subharmonic OPO combs are phase locked to the pump and their teeth (e.g. if $\Delta N = 2$ and $N_{1,2}$ are even) overlap at the anchor point ‘C’ distanced by $f_{ceo}/2$ from zero, and at a common anchor point ‘D’ ($\lambda \approx 3.13 \mu\text{m}$). (c) RF-to-optical frequency mapping for $\Delta N = 2$ and $\Delta N = 8$.

Discussion

Using a highly-coherent and broadband dual-comb spectroscopy system based on subharmonic generation, we demonstrate the acquisition of up to 2.5 million spectral elements over the wavelength range of 3.17–5.13 μm (frequency span 1200 cm^{-1})—by interleaving spectra with discretely stepped comb-line spacing. Among other molecular absorption features, we fully resolved the Doppler-broadened spectra corresponding to the strongest 981 transitions of the $\nu_1 + \nu_3$ band (4.5–4.7 μm) of CS_2 and its three isotopologues with ~ 50 -kHz accuracy of the absolute frequency referencing. Most of the line intensities were accurately measured for the first time and will be included in the line lists for molecular databases⁴³. Furthermore, the obtained data can be used as a testing ground for theoretical models. The sampling point spacing in our experiment can be further reduced (at the expense of the measurement time) by 2–3 orders of magnitude, limited only by the 50-kHz uncertainty in the absolute frequency. This in turn can be further improved using a more stable narrow-linewidth optical reference laser and a tighter feedback loop.

Methods

OPO comb modes and RF-to-optical frequency mapping. The comb modes for both Tm-fiber pump lasers were locked, at the two common anchor points (Fig. 6): near zero frequency with a common carrier-envelope offset (CEO) $f_{ceo}^{pump} = +190 \text{ MHz}$ (point A), and near the frequency of a narrow-linewidth ($\sim 3 \text{ kHz}$) continuous wave (CW) reference ‘RIO’ semiconductor laser at near $\lambda \approx 1564 \text{ nm}$ with an offset $f_{RIO} = +140 \text{ MHz}$ (point B). Between A and B, there are N_1 intermodal intervals (f_{r1}) for laser 1 and N_2 intervals ($f_{r2} > f_{r1}$) for laser 2, such that $N_1 \times f_{r1} = N_2 \times f_{r2}$ and

$$\Delta f_r = f_{r2} - f_{r1} = \frac{N_1 - N_2}{N_2} f_{r1} = \frac{\Delta N}{N_2} f_{r1} = \frac{\Delta N}{N_1} f_{r2}. \quad (1)$$

The repetition rate offset Δf_r between the two lasers is quantized. For example, for $\Delta N = 2$, $\Delta f_r \approx 138.5 \text{ Hz}$ and for even $N_{1,2}$ such that $N_1 = 2(k_0 + 1)$ and $N_2 = 2k_0$ with k_0 an integer, the ratios $f_{r1}/\Delta f_r$ and $f_{r2}/\Delta f_r$ are integer numbers. In fact, in our experiments the measured ratio $f_{r1}/\Delta f_{rep} (\approx k_0)$ was an integer: 831,844 with a remainder after division $< 10^{-3}$.

Both OPO combs were running in the frequency-divide-by-2 mode with respect to the pump, such that that CEO frequency for both of them (anchor point C in Fig. 6 was half of that of the pump CEO:

$$f_{ceo}^{OPO1} = f_{ceo}^{OPO2} = \frac{1}{2}f_{ceo}^{pump}. \quad (2)$$

Another anchor point (D) is at $\nu_D = \frac{1}{2}\nu_B$ (near $\sim 3.13 \mu\text{m}$), just above (in frequency) our broadest spectral span. For $\Delta N = 2$ we used the following RF-to-optical mapping for the sensing comb:

$$\nu = \nu_D - \frac{f_{r2}}{\Delta f_r}f = \frac{1}{2}f_{ceo}^{pump} + \frac{f_{r2}}{\Delta f_r}(f_{r1} - f), \quad (3)$$

where ν is the optical frequency that interrogates the sample, and f is RF frequency. The whole 1200 cm^{-1} spectral span is thus mapped to the 1–48-MHz RF range. In a similar way, with the reduced ($2030\text{--}2300 \text{ cm}^{-1}$) frequency coverage, selected for the study of CS_2 molecule, we have used $\Delta N = 8$, $\Delta f_r = 554 \text{ Hz}$, such that the RF comb's span matches the aliasing free bandwidth, with the following RF-to-optical frequency mapping for the sensing comb:

$$\nu = \frac{1}{2}f_{ceo}^{pump} + \frac{f_{r2}}{\Delta f_r}(3f_{r1} - f). \quad (4)$$

Here, the term $\frac{1}{2}f_{ceo}^{pump} + 3\frac{f_{r1}f_{r2}}{\Delta f_r}$ corresponds to the anchor point “E” in Fig. 6c for both OPO combs, and $\frac{f_{r2}}{\Delta f_r}$ is the RF-to-optical upscaling factor (with a negative sign).

Remarkably, with the known ΔN , frequency offsets f_{ceo}^{pump} and f_{RIO} , and with just two readings from the frequency counters (f_{r1} and Δf_r), we were able to determine the vacuum wavelength of the RIO laser with the fractional accuracy of better than 10^{-9} .

Stabilization and stepping of the RIO laser and the absolute frequency referencing. Since the two pump Tm-fiber combs are phase locked to a common optical reference (RIO laser), and the OPO combs, in turn, are phase-locked to the Tm combs, the drifts of the RIO laser frequency (ν_{RIO}), typically $\sim 10 \text{ MHz}$ during a day, affect the absolute position of the comb lines. To avoid these drifts, we implemented an active ν_{RIO} stabilization. Using the readings of a frequency counter referenced to a Rb clock for the repetition rate (f_{r1}) of one of the Tm-fiber combs, and applying the difference between the measured and a desired repetition rate as a feedback to act on the RIO laser temperature with a slow servo loop with an update time of 4 s, we achieved the standard deviation for f_{r1} of 0.09 Hz ($\sigma_{f_{r1}}/f_{r1} = 7.8 \times 10^{-10}$), which corresponds to the standard deviation of the RIO laser frequency $\sigma_{\nu_{RIO}} = \nu_{RIO} \times \sigma_{f_{r1}}/f_{r1} \approx 150 \text{ kHz}$. Since both OPO combs are pinned to a common frequency offset near zero, the frequency uncertainty of a comb line is proportional to its absolute frequency. For example, for the CS_2 absorption band near $4.6\text{-}\mu\text{m}$, the standard deviation is $\sigma\nu = \nu \times 7.8 \times 10^{-10} \approx 50 \text{ kHz}$.

The interleaved DCS spectra were acquired by stepping, through temperature control, ν_{RIO} in eight 42.35-MHz increments (corresponding to f_{r1} steps of $\approx 25 \text{ Hz}$), resulting in the comb-line shifts that vary from 21 MHz (at $\approx 3.2 \mu\text{m}$) to 13 MHz (at $\approx 5.1 \mu\text{m}$), and were 14.4 MHz (about 1/8 of the original 115-MHz comb-line spacing) near the $4.6\text{-}\mu\text{m}$ absorption band of CS_2 .

CS_2 sample preparation. A droplet of liquid-phase CS_2 dissolved in n-hexane at a concentration of $100.6 \mu\text{g/ml} \pm 2\%$ (Chem Services, Inc.) was placed in a 10-ml-volume chemical flask and fully evaporated, together with the ambient room air in the headspace, into the evacuated 0.5-L multipass gas cell. The resulting pressure in the gas cell was then measured with an accuracy of $\pm 1\%$. Next, the same procedure was repeated with the chemical flask filled just with room air. The fractional (by molecules) concentration of the hexane- CS_2 mixture in the gas cell was determined by comparing the measured pressure in the gas cell due to the mixture (liquid droplet plus air) and the pressure produced due to the flask filled just with air. (In fact, there were comparable concentrations of molecules coming from the droplet and room air.) For spectral measurements, the gas cell was further evacuated to get the total pressure of 6.03 mbar, with the calculated CS_2 concentration of $94.6 \text{ ppm} \pm 3\%$ (part-per-million by volume). The gas cell temperature was kept at $293.7 \pm 0.5 \text{ K}$.

Received: 2 July 2020; Accepted: 12 October 2020

Published online: 29 October 2020

References

- Schliesser, A., Picqué, N. & Hänsch, T. W. Mid-infrared frequency combs. *Nat. Photon.* **6**, 440 (2012).
- Picqué, N. & Hänsch, T. W. Frequency comb spectroscopy. *Nat. Photon.* **13**, 146–157 (2019).
- Coddington, I., Swann, W. C. & Newbury, N. R. Coherent multiheterodyne spectroscopy using stabilized optical frequency combs. *Phys. Rev. Lett.* **100**, 013902 (2008).
- Coddington, I., Swann, W. C. & Newbury, N. R. Time-domain spectroscopy of molecular free-induction decay in the infrared. *Opt. Lett.* **35**, 1395–1397 (2010).
- Zolot, M. *et al.* Direct-comb molecular spectroscopy with accurate, resolved comb teeth over 43 THz. *Opt. Lett.* **37**, 638–640 (2012).
- Yan, M. *et al.* Mid-infrared dual-comb spectroscopy with electro-optic modulators. *Light Sci. Appl.* **6**, e17076 (2017).
- Ycas, G. *et al.* High-coherence mid-infrared dual-comb spectroscopy spanning 2.6 to 5.2 μm . *Nat. Photon.* **12**, 202–209 (2018).
- Muraviev, V., Smolski, V. O., Loparo, Z. E. & Vodopyanov, K. L. Massively parallel sensing of trace molecules and their isotopologues with broadband subharmonic mid-infrared frequency combs. *Nat. Photon.* **12**, 209–214 (2018).
- Schiller, S. Spectrometry with frequency combs. *Opt. Lett.* **27**, 766 (2002).
- Baumann, E. *et al.* Spectroscopy of the methane ν_3 band with an accurate midinfrared coherent dual-comb spectrometer. *Phys. Rev. A* **84**, 062513 (2011).

11. Coddington, A., Newbury, N. & Swann, W. Dual-comb spectroscopy. *Optica* **3**, 414–426 (2016).
12. Weichman, M. L. *et al.* Broadband molecular spectroscopy with optical frequency combs. *J. Molec. Spectrosc.* **355**, 66–78 (2019).
13. Jacquet, P., Mandon, J., Bernhardt, B., Holzwarth, R., Guelachvili, G., Hänsch, T. W. & Picqué, N. Frequency comb Fourier transform spectroscopy with kHz optical resolution, in *Advances in Imaging, OSA Technical Digest (Optical Society of America, 2009)*, paper FMB2.
14. Rutkowski, L. *et al.* Sensitive and broadband measurement of dispersion in a cavity using a Fourier transform spectrometer with kHz resolution. *Opt. Express* **25**, 21711 (2017).
15. Villares, G., Hugi, A., Blaser, S. & Faist, J. Dual-comb spectroscopy based on quantum-cascade-laser frequency combs. *Nat. Commun.* **5**, 5192 (2014).
16. Gianella, M., Nataraj, A., Tuzson, B., Jouy, P., Kapsalidis, F., Beck, M., Mangold, M., Hugi, A., Faist, J., & Emmenegger, L. High-resolution and gapless dual comb spectroscopy with current-tuned quantum cascade lasers. [arXiv:1910.13973](https://arxiv.org/abs/1910.13973) (2019).
17. Rothman, L. S. *et al.* The HITRAN 2008 molecular spectroscopic database. *J. Quant. Spectrosc. Radiat. Transf.* **110**, 533–572 (2009).
18. Yu, M., Okawachi, Y., Griffith, A. G., Lipson, M. & Gaeta, A. L. Microresonator-based high-resolution gas spectroscopy. *Opt. Lett.* **42**, 4442 (2017).
19. Ideguchi, T., Poisson, A., Guelachvili, G., Picqué, N. & Hänsch, T. W. Adaptive real-time dual-comb spectroscopy. *Nat. Commun.* **5**, 3375 (2014).
20. Roy, J., Deschênes, J.-D., Potvin, S. & Genest, J. Continuous real-time correction and averaging for frequency comb interferometry. *Opt. Express* **20**, 21932–21939 (2012).
21. Guay, P. *et al.* Toward free-running operation of dual-comb fiber lasers for methane sensing. *Appl. Opt.* **59**, B35 (2020).
22. Burghoff, D., Yang, Y. & Hu, Q. Computational multiheterodyne spectroscopy. *Sci. Adv.* **2**(11), e1601227 (2016).
23. Sterczewski, L. A. *et al.* Multiheterodyne spectroscopy using interband cascade lasers. *Opt. Eng.* **57**(1), 011014 (2017).
24. Vodopyanov, K. L., Wong, S. T. & Byer, R. L. Infrared frequency comb methods, arrangements and applications. U.S. patent 8,384,990 (February 26, 2013).
25. Leindecker, N., Marandi, A., Byer, R. L. & Vodopyanov, K. L. Broadband degenerate OPO for mid-infrared frequency comb generation. *Opt. Express* **19**, 6304–6310 (2011).
26. Leindecker, N. *et al.* Octave-spanning ultrafast OPO with 2.6–6.1 μm instantaneous bandwidth pumped by femtosecond Tm-fiber laser. *Opt. Express* **20**, 7047–7053 (2012).
27. Ru, Q. *et al.* Self-referenced octave-wide subharmonic GaP optical parametric oscillator centered at 3 μm and pumped by an Er-fiber laser. *Opt. Lett.* **42**, 4756–4759 (2017).
28. Smolski, V. *et al.* Half-Watt average power femtosecond source spanning 3–8 μm based on subharmonic generation in GaAs. *Appl. Phys. B* **124**, 101 (2018).
29. Vainio and Karhu. Fully stabilized mid-infrared frequency comb for high-precision molecular spectroscopy. *Opt. Express* **25**, 4190 (2017).
30. Loparo, Z. E., Ninnemann, E., Ru, Q., Vodopyanov, K. L. & Vasu, S. S. Broadband mid-infrared optical parametric oscillator for dynamic high-temperature multi-species measurements in reacting systems. *Opt. Lett.* **45**, 491–494 (2020).
31. Marandi, A., Leindecker, N. C., Vodopyanov, K. L. & Byer, R. L. All-optical quantum random bit generation from intrinsically binary phase of parametric oscillators. *Opt. Express* **20**, 19322–19330 (2012).
32. Marandi, A., Wang, Z., Takata, K., Byer, R. L. & Yamamoto, Y. Network of time-multiplexed optical parametric oscillators as a coherent Ising machine. *Nat. Photon.* **8**, 937–942 (2014).
33. Marandi, A., Ingold, K. A., Jankowski, M. & Byer, R. L. Cascaded half-harmonic generation of femtosecond frequency combs in the mid-infrared. *Optica* **3**, 324–327 (2016).
34. Marandi, A., Leindecker, N., Pervak, V., Byer, R. L. & Vodopyanov, K. L. Coherence properties of a broadband femtosecond mid-IR optical parametric oscillator operating at degeneracy. *Opt. Express* **20**, 7255–7262 (2012).
35. Lee, K. F. *et al.* Midinfrared frequency combs from coherent supercontinuum in chalcogenide and optical parametric oscillation. *Opt. Lett.* **39**, 2056–2059 (2014).
36. Smolski, V. O., Yang, H., Gorelov, S. D., Schunemann, P. G. & Vodopyanov, K. L. Coherence properties of a 2.6–7.5 μm frequency comb produced as a subharmonic of a Tm-fiber laser. *Opt. Lett.* **41**, 1388 (2016).
37. Wan, C., Li, P., Ruehl, A. & Hartl, I. Coherent frequency division with a degenerate synchronously pumped optical parametric oscillator. *Opt. Lett.* **43**, 1059 (2018).
38. Yang, C., Deng, H., Qian, Y., Li, M., Chen, B., Xu, Z., & Kan, R. Absorption lines measurements of carbon disulfide at 4.6 μm with quantum cascade laser absorption spectroscopy. *Spectrochim. Acta* **225**, 117478 (2020).
39. Landis, G. A. Astrobiology: the case for Venus. *J. Br. Interplanetary Soc.* **56**, 250 (2003).
40. Phillips, M., Sabas, M. & Greenberg, J. Increased pentane and carbon disulfide in the breath of patients with schizophrenia. *J. Clin. Pathol.* **46**, 861 (1993).
41. Sehnert, S. S., Jiang, L., Burdick, J. F. & Risby, T. H. Breath biomarkers for detection of human liver diseases: preliminary study. *Biomarkers* **7**, 174 (2002).
42. Eilers, P. H. C. A perfect smoother. *Anal. Chem.* **75**(14), 3631–3636 (2003).
43. Karlovets, E. V., Gordon, I. E., Konnov, D., Muraviev, A. & Vodopyanov, K. L. Dual-comb laser spectroscopy of CS₂ near 46 μm . *J. Quant. Spectrosc. Radiat. Transf.* **256**, 107269 (2020).
44. Zeng, Z., Altarawneh, M. & Dlugogorski, B. Z. Atmospheric oxidation of carbon disulfide (CS₂). *Chem. Phys. Lett.* **669**, 43 (2017).

Acknowledgements

We acknowledge support from the Office of Naval Research (ONR), Grant Number N00014-15-1-2659 and from the Defense Advanced Research Projects Agency (DARPA), Grant Number W31P4Q-15-1-0008. We thank Ekaterina Karlovets and Iouli Gordon for helping with the analysis of the CS₂ spectra, and Peter Schunemann for providing nonlinear-optical OP-GaAs crystals.

Author contributions

A.V.M. constructed the experimental setup. D.K. developed the algorithm for data acquisition and processing. A.V.M. and D.K. carried out the measurements and analyzed the data. K.L.V. initiated and supervised the project; he also analyzed the data and wrote the paper.

Competing interests

The authors declare no competing interests.

Additional information

Correspondence and requests for materials should be addressed to K.L.V.

Reprints and permissions information is available at www.nature.com/reprints.

Publisher's note Springer Nature remains neutral with regard to jurisdictional claims in published maps and institutional affiliations.



Open Access This article is licensed under a Creative Commons Attribution 4.0 International License, which permits use, sharing, adaptation, distribution and reproduction in any medium or format, as long as you give appropriate credit to the original author(s) and the source, provide a link to the Creative Commons licence, and indicate if changes were made. The images or other third party material in this article are included in the article's Creative Commons licence, unless indicated otherwise in a credit line to the material. If material is not included in the article's Creative Commons licence and your intended use is not permitted by statutory regulation or exceeds the permitted use, you will need to obtain permission directly from the copyright holder. To view a copy of this licence, visit <http://creativecommons.org/licenses/by/4.0/>.

© The Author(s) 2020